https://doi.org/10.5194/egusphere-2026-508
Preprint. Discussion started: 27 February 2026

A numerical framework for modeling iceberg calving and ice-front migration of grounded glacier tongues

Veena Prasad[1], Oskar Herrmann[1], Ilaria Tabone[2], Mamta K C[1], Alexander R. Groos[1], Guillaume Jouvet[3], James R. Jordan[4], and Johannes J. Fürst[1]

[1]Institute of Geography, Friedrich-Alexander-Universität Erlangen-Nürnberg, Germany
[2]Department of Geophysics, University of Concepción, Concepción, Chile
[3]Institute of Earth Surface Dynamics, University of Lausanne, Lausanne, Switzerland
[4] Department of Geography, Swansea University, Swansea, United Kingdom

Correspondence: Veena Prasad (veena.prasad@fau.de)

Abstract. Marine- and lake-terminating glaciers, though limited in number, are important contributors to global sea-level rise. Their mass budget is governed by surface mass balance and frontal ablation. The latter remains poorly constrained in glacier models as calving involves processes that act on various spatial and temporal scales. In this manuscript, we present the integration of a subgrid-scale ice-front tracking method based on the level-set method, coupled with a strain-based calving criterion, into the Instructed Glacier Model. The framework is applied to a synthetic glacier setup initially to exemplify code sanity, reversibility, and shape preservation. For this experiment, the integration of both a re-initialization scheme and an informed extrapolation of frontal velocities was key. We also extended the approach to allow for frontal advance of grounded ice tongues. To further enhance the approach, we incorporated a thickness scheme that dynamically adjusts the frontal thickness, permitting the frontal advance of grounded ice tongues while maintaining consistency with mass conservation throughout geometric evolution. The framework is subsequently applied to a real-world setting, where the model is calibrated and evaluated using five marine-terminating glaciers in Kongsfjorden, Svalbard. The results show that the model can capture both the magnitude and spatial variability of calving front retreat. We therefore deem our implementation as a versatile method to track ice fronts of grounded glacier tongues. This scheme enables an adequate quantification of atmospheric and oceanic influences on current and future ice loss of marine-terminating glaciers.

1 Introduction

Since the 1970s, there has been a pronounced increase in mass loss from glaciers worldwide, making them a major contributor to current sea-level rise (Zemp et al., 2019; Hugonnet et al., 2021; Dussaillant et al., 2025). Among these, the marine- and lake terminating (MALT) glaciers experience the most rapid changes due to interactions at both the atmospheric and water interfaces (Wouters et al., 2019; GlaMBIE Team, 2025). Mass loss from MALT glaciers is controlled by two main factors: the surface mass balance and frontal ablation. Surface mass balance comprises all processes at the glacier surface that govern mass gain or loss. Frontal ablation is defined as the mass loss at the ice front of the glacier tongue. It includes iceberg calving, sub-aerial melting, sublimation, and sub-aqueous melting (Cogley et al., 2010; Pope et al., 2012). Both factors are critical for

https://doi.org/10.5194/egusphere-2026-508
Preprint. Discussion started: 27 February 2026

the overall mass budget of MALT glaciers. Regional estimates indicate that frontal ablation dominates the overall glacier mass loss in many fast-retreating regions (Kochtitzky et al., 2022a, b). For instance, for glaciers on Greenland, frontal ablation alone contributed to 559±13 Gt a^{-1} from 2010 to 2020 (Kochtitzky et al., 2023), while the overall mass loss is estimated only as 286 ± 20 Gt a^{-1} for a largely overlapping period (2010-2018) (Mouginot et al., 2019). Similarly, in regions such as Alaska, High Mountain Asia, and Svalbard, frontal ablation is becoming increasingly important in the total glacier mass budget (Recinos et al., 2019). However, both observational and modeled estimates of frontal ablation remain limited to a few individual glaciers or regions, largely due to the complex and dynamic nature of the glacier calving front. Furthermore, an insufficient knowledge of accurate glacier bed topography and ice thickness near the terminus exists for water terminating glaciers (Fürst et al., 2024). Many existing studies rely on ice discharge approximations for frontal ablation, which often overlook the influence of iceberg calving and variations in the calving front position. Future calving losses thus contribute significantly to the uncertainty in predictions of sea-level rise (Li et al., 2023)

Explicitly representing calving front dynamics in glacier evolution modeling is necessary to address these limitations. However, accurately modeling calving processes remains challenging due to the complex interactions among stress, geometry, and external forcings (Benn et al., 2007). Recent advances in calving research have incorporated a variety of empirical and physically based calving frameworks into ice-flow models. These frameworks are generally categorized as either assuming a steady-state calving front geometry or incorporating a dynamically evolving calving front, with the latter constituting the focus of this study. Most of the existing research is on rapidly changing tidewater glaciers. Often, the calving front dynamics of the freshwater glaciers have received comparatively little attention, despite exhibiting patterns and variability similar to marine-terminating glaciers (Pfeffer, 2000; Nick et al., 2013; Shugar et al., 2020; Compagno et al., 2022; Vacek et al., 2025). Incorporating lake-terminating glaciers in calving models requires additional attention, as increased glacier retreat causes formation and expansion of proglacial lakes (Minowa et al., 2023).

Calving is primarily controlled by an interplay of multiple dynamic processes at the glacier terminus, including stretching and fracture initiation and crevasse propagation, imbalance between cryostatic and hydrostatic pressures, submarine undercutting of frontal ice cliff, and buoyant forces at the terminus (Benn et al., 2007). Sudden episodic removal of ice at the glacier front can substantially affect the glacier stress balance and flow regime (Amundson et al., 2022). As ice is lost by calving, its previous restraining force on the upstream ice is lowered or lost. An immediate consequence of reduced buttressing can be flow acceleration at the terminus. This acceleration can then lead to further thinning upstream while the glacier readjusts (Mitcham et al., 2022). In addition, the presence of water at the terminus typically increases ice velocity near the terminus by reducing effective pressure. Higher velocities can further act as a feedback mechanism for calving events. While increased velocity and retreat are key factors, basal drag, lateral drag, and longitudinal stress gradients also control glacier flow and consequently calving rates. Physics-based calving models (Nick et al., 2009; Morlighem et al., 2016) and process-based formulations (Benn et al., 2007) provide valuable insight into calving dynamics at high spatial and temporal resolution. Several empirical calving relations have been formulated and implemented in glacier evolution models, many of which relate calving rate to terminus velocity, water depth, crevasse propagation, or glacier stress and strain rates (Brown et al., 1983; van der Veen, 1996; Pfeffer et al., 1997; Levermann et al., 2012). These empirical approaches are found to be effective for accurately estimating the

https://doi.org/10.5194/egusphere-2026-508
Preprint. Discussion started: 27 February 2026

calving rate with proper calibration (Choi et al., 2018; Wilner et al., 2023). Recent studies also incorporate dynamically evolving calving fronts along with the physics-based calving law. A widely used approach is to track the calving front along the flowline, simplifying the terminus' complex geometry into a 1D representation (Vieli and Nick, 2011; Nick et al., 2009). However, the accuracy of this method is subject to parameterizations. Moreover, 1D methods are ineffective in tackling the complex topology of the calving front and fail to resolve lateral variations. Consequently, there is a pressing demand for more accurate representation of calving-front dynamics in prognostic models of MALT glacier evolution. The level-set method (LSM), introduced by Osher and Sethian (1988), has been used recently in many ice flow models to implicitly track the calving front (Bondzio et al., 2016; Morlighem et al., 2016; Choi et al., 2018). The LSM is a numerical technique based on partial differential equations to implicitly represent and track evolving interfaces. Although its application in glacier modeling is still developing, studies indicate that LSM is well suited for resolving the intricate geometry and dynamic adjustments of the calving front (Pralong and Funk, 2004; Bondzio et al., 2016; Morlighem et al., 2016). LSM is found to be effective in tracking complex topological changes, making it suitable for tracking the calving front propagation. However, the method is subject to numerical instabilities that require mass conservation and re-initialization at frequent intervals (Cheng et al., 2024). Recent advances show that the LSM can be seamlessly integrated into finite-element ice-flow models, enabling glacier-specific calving-front tracking. (Bondzio et al., 2016; Cheng et al., 2024; Badgeley et al., 2025; Barnes et al., 2026). Recent efforts increasingly focus on refining physically based calving laws and the parameter calibration within dynamically consistent frameworks.

The main objective of this study is to establish a calving framework suitable for regional-scale application to understand the future evolution of MALT glaciers. We present the implementation of the method in the Instructed Glacier Model (IGM) (Jouvet et al., 2022), a Python-based modeling tool to efficiently simulate glacier evolution on various scales. The whole framework is tested using synthetic glacier domain. The method was further calibrated across five glaciers in Svalbard to reconstruct the calving front for the period 2014 to 2024, to showcase its applicability to a real-world scenario. The Svalbard glaciers are of particular importance, due to the regions' amplified Arctic warming (Schuler et al., 2025) and their significant contribution to sea level rise (Nuth et al., 2010).

2 Data and Methods

2.1 The framework for calving and ice-front migration

In this section, we present the implementation of the calving algorithm, along with the ice-flow model coupled with it. The calving algorithm consists of two key components: a sub-grid front tracking framework and a physics-based calving law. Our sub-grid front tracking framework is adapted from the LSM used in the Kori-ULB ice flow model (Pattyn, 2017; Coulon et al., 2024). We extend this approach by incorporating re-initialization, physically consistent velocity-extension and eigen calving. Furthermore, we implement a front-thickness update scheme to make the level set module suitable for coupling with a glacier evolution model, particularly during glacier advance phases.

https://doi.org/10.5194/egusphere-2026-508
Preprint. Discussion started: 27 February 2026

2.1.1 Glacier dynamics and surface mass balance

Glacier mass balance and evolution is simulated using IGM V.2 (Jouvet et al., 2022). For ice dynamics, we do not rely on the emulated velocities from IGM but rather rely on the solution of the built-in classical solver (Jouvet et al., 2022). The surface mass balance (SMB) is estimated as a function of elevation (z) using three parameters: time-evolving equilibrium line altitude (z_{ELA}), ablation gradient (β_{abl}), and accumulation gradient (β_{acc}). Using numerical optimization, the horizontal velocity components are estimated using the classic solver, built-in IGM, which is based on the Blatter-Pattyn approximation. Finally, ice thickness is updated by solving the mass conservation equation that integrates ice flow and surface mass balance.

$$\frac{\partial h}{\partial t} + \nabla U \cdot h = SMB. \tag{1}$$

The mass conservation equation is discretized using an explicit first-order upwind finite-difference scheme on the 2D grid. In this scheme, ice is transferred between adjacent grid cells based on edge-defined fluxes.

2.1.2 Level-set Method (LSM)

In the current implementation, we use an implicit finite difference scheme to evolve the level set. The LSM relies on a signed distance function to represent evolving interfaces. The level set function $(\phi(x,t))$ at a given point in space (x) and time (t) is initialized with the interface, i.e. the calving front, defined as the zero contour. The remaining nodes of the domain are populated using a fast marching method, which extends the signed distance function outward from the front, ensuring that the magnitude of the first derivative of the distance function is one ($\mid \nabla\phi \mid = 1$). The sign of ϕ defines whether the region is ice-(Ω_i) or ocean-covered (Ω_c) as follows:

$$\phi(x,t) = \begin{cases} > 0 & \text{for } x \in \Omega_c, \\ < 0 & \text{for } x \in \Omega_i, \\ = 0 & \text{for } x \in \Omega_f, \end{cases} \tag{2}$$

where, (Ω_f) is the interface or calving front. Differentiating Eq. 2 in time and applying the chain rule, we obtain:

$$\frac{\partial \phi}{\partial t} + v_f . \nabla \phi = 0, \tag{3}$$

where v_f is the front velocity of the level set, which is the difference between the ice velocity (v) and the calving rate (c). The velocity components should be perpendicular to the ice-front.

$$v_f = (v - c) \cdot \hat{n}. \tag{4}$$

In order to solve Eq. (3), the frontal speed (v_f) must be extended over the entire computational domain or at least over a band of neighboring nodes (narrow band approach) (Adalsteinsson and Sethian, 1999; Xue et al., 2021). In our implementation, we use the narrow band approach for solving the level set and velocity extension. The velocity is extended in the narrow band so

https://doi.org/10.5194/egusphere-2026-508
Preprint. Discussion started: 27 February 2026

that it does not change along the normal direction but can vary along the interface itself. The extended velocity (v_f^{ext}) of the domain is estimated to satisfy the following condition:

$$\nabla v_f^{ext}.\nabla\phi = 0. \tag{5}$$

This method ensures that the advection of neighboring nodes is consistent with the interface evolution (Adalsteinsson and Sethian, 1999). Limiting the level set advection and velocity extension only to the narrow band, reduces the computational cost of the entire implementation.

2.1.3 Calving rate

The calving rate of the glacier is estimated using the eigen calving proposed by Levermann et al. (2012). The eigen calving has been widely adopted in large-scale ice-sheet and outlet-glacier modeling studies due to its ability to capture first-order calving dynamics based solely on kinematic fields (Martin et al., 2011; Wilner et al., 2023). The eigen calving framework provides a physically based approach, deriving calving rate from the principal components of the strain rate. Eigen calving defines the calving rate as a function as follows:

$$c = K_{ec}.\epsilon_{\parallel}.\epsilon_{\perp}, \tag{6}$$

where ($\epsilon_{\parallel}$) is the along-flow strain rate and ($\epsilon_{\perp}$) is the across-flow strain rates and K_{ec} is the calibration constant (K_{ec}) and is assumed to represent the physical properties influencing calving.

2.1.4 Level set re-initialization

Over time, as the interface evolves, the value of level set will deviate from the true signed distance function, which may cause numerical instabilities, affecting the evolution of the interface. Re-initialization of the level set is periodically employed to restore the signed distance function, while the interface (zero level set) remains unchanged (Sussman et al., 1994). This ensures that the zero level set is accurately tracking the evolving calving front on a subgrid length scale. In the current implementation, re-initialization is performed by solving the following partial differential equation:

$$\frac{\partial\phi}{\partial T} = sign(\phi_0)(1 - |\nabla\phi|) \tag{7}$$

where T is the pseudo-timestep for re-initialization, ϕ_0 is the original level set, and $\frac{\partial\phi}{\partial T}$ drives ϕ towards a signed distance function without altering the zero level set. The partial difference equation based re-initialization has the ability to handle complex shapes and is ideal for frequent re-initialization, which is often necessary (Bondzio et al., 2016; Morlighem et al., 2016). Without re-initialization, the gradient norm $|\nabla\phi|$ deviates from 1, smearing the interface and signed distance function. The control parameters for Eq. (7) are finalized after testing on synthetic level set and glacier setups. There is no optimal value for the re-initialization time step. Thus, in our study, we use the same time step for re-initialization as for time evolution in IGM (Eq.1).

https://doi.org/10.5194/egusphere-2026-508
Preprint. Discussion started: 27 February 2026

2.1.5 Ice front advance

As the glacier calving front propagates, the ice thickness and surface topography must be updated at each timestep based on the level-set value. Eq. (8) shows the classification of each cell based on the value of the level set.

$$\begin{cases} \phi_{i,j} < 0 & \text{ice-covered} \\ \phi_{i,j} \geq 0 & \text{water filled} \end{cases} \tag{8}$$

On the newly formed fully ice covered cells, the surface topography and ice thickness is updated based on the values extracted from its neighboring ice filled cells. The ice thickness is extracted from the neighboring ice-covered cell, assuming that the surface topography remains similar to the immediate upstream cells. We take the minimum surface topography from the immediate upstream neighbor cells for this purpose. This ensures that the thickness distribution remains consistent with the previous calving front positions. The glacier and synthetic setup used in this study is always assumed to be grounded, and thickness is estimated as the difference between newly added surface and local bed elevation. In addition, ice must be fully removed from a water filled cell, as glacier retreats. The proposed method integrates seamlessly with the mass transport modules of the IGM (Eq.1), preserving compatibility with its thickness and velocity fields.

2.2 Synthetic glacier domain

Two different synthetic test domains were used to evaluate the robustness of the model in this study. These synthetic domains allow us to assess mass conservation, symmetry preservation, and accuracy of initialization and re-initialization. The first domain is a simple 2-D domain with a circular interface, which serves as a baseline numerical experiment. Details of this experiment are provided in the appendix (Sect. A). This section focuses on the application of the LSM on an idealized synthetic glacier geometry setup using IGM. This geometry enables a controlled environment to further test the numerical stability, and the ability of the current implementation to handle simplified but realistic glacier-like features before extending to the real-world scenario. Furthermore, we use this setup to evaluate the reversibility of the glacier advance and retreat within the LSM framework.

The computational domain is structured as a 2-D grid with a size of 20 km by 10 km having a resolution of 200 m. The glacier bed topography is defined using a combination of slope profile in the x-direction and a parabolic profile in the y-direction to imitate valley-like features (Fig 1). The bed topography of the synthetic setup is prescribed as:

$$\mathrm{topg}(x,y) = -\tan\left(0.4\pi \frac{x - x_c}{x_c}\right) \tan(\alpha)\, x_c + \frac{(y-5000)^2}{50000} + 3250, \tag{9}$$

where, α is the slope and x_c defines the mid-section of the computational domain as:

$$x_c = \frac{1}{2}\, n_x\, dx. \tag{10}$$

At the lateral domain edges (600 m in each side), periodic boundary conditions are employed. At the inflow boundary, velocities and thickness values are set to zero (Dirichlet condition). The bed topography is constrained to a minimum of 10

https://doi.org/10.5194/egusphere-2026-508
Preprint. Discussion started: 27 February 2026

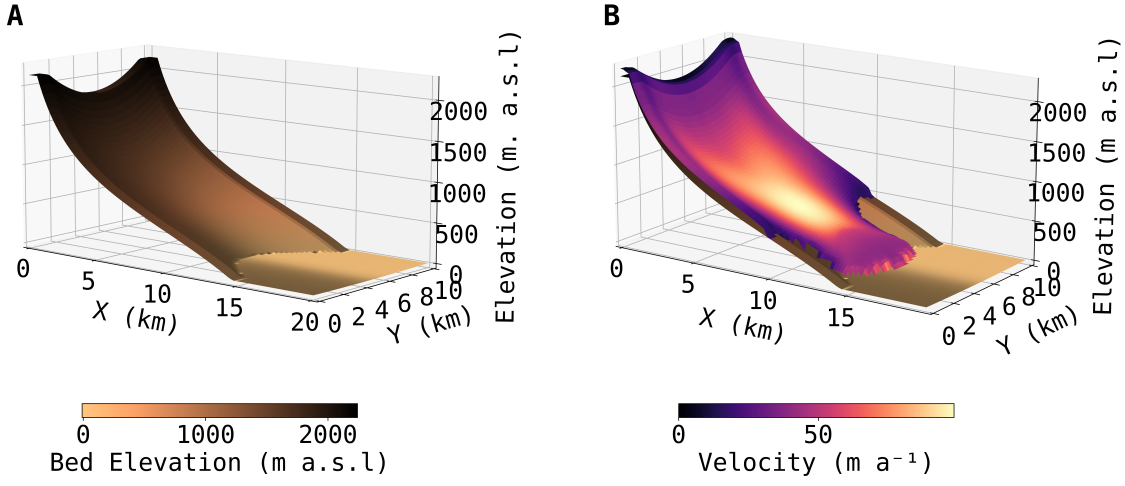

Figure 1. Spatial distribution of (A) initial bed topography and (B) glacier velocity of the synthetic domain generated through a 125 year model run of IGM. The synthetic glacier domain has an 'ice covered' area of 180 km^2 and an ice volume of 26.3 km^3.

m below sea-level to avoid excessively thick fronts during advance. The bed topography below zero is treated as ocean/water, thereby allowing us to treat the synthetic domain as a MALT glacier.

Concerning the SMB, a simple elevation-dependent parametrization is used with a constant equilibrium line altitude (200 m. a. s. l.) along with vertical gradients of ablation (0.09 m w. e. a^{-1} m^{-1}) and accumulation (0.05 m w. e. a^{-1} m^{-1}). For model initialization, we pursued a 125-year simulation, allowing ice to advance into the 'water domain'. The model domain does not reach a full equilibrium state in terms of thickness and velocity evolution. However, the overall thickness and velocity distribution provides a sufficiently stable configuration for subsequent level-set applications. In the model, we do not allow flotation. All ice is treated as grounded.

The calving front, positioned at the ocean boundary, spanned 8.5 km in width. The synthetic glacier shows rather thin ice at the calving front. To ensure that the initial geometry shows a more realistic ice cliff at the glacier front, we first impose a constant frontal velocity v_f = 200 m a^{-1} (Eqn. 3), for 2 years to cut back the margin position. From here onward, we refer to this extent as the initial geometry of the synthetic domain (Fig.1B). The simulation period can be divided into two phases: the advance phase (t = 1 to 12 years) and the retreat phase (t = 13 to 32 years). During the advance phase, a constant velocity of 400 m a^{-1} in x-direction is applied at the level set interphase, resulting in steady frontal advance for 12 years. Thereafter, v_f is inverted to -400 m a^{-1} for the next 22 years to simulate glacier front retreat. The retreat phase is used to test the reversibility of the method. As the glacier advances, the SMB values are kept zero at the terminus to ensure that the glacier domain does not

https://doi.org/10.5194/egusphere-2026-508
Preprint. Discussion started: 27 February 2026

grow or remove mass at the terminus. The ice thickness at the calving front is thus exclusively updated based on the level set evolution (Sect. 2.1.5). While IGM updates the thickness and velocity fields where ice is present and in areas above sea-level, the LSM controls the advance and retreat at the marine interface.

2.3 Real-world experiment

An overview of implementation of the calving module and integration with IGM is given in Fig. 2. The workflow presents the inclusion of Sect. 2.1 with IGM. In addition to this, the real-world experiments also include calibration of glacier velocity and the calving parameter, K_{ec}, which is described in Sect. 2.3.2.

2.3.1 Data

We selected five tidewater glaciers located at the southern end of Kongsfjorden in the Svalbard archipelago (Fig. 3): Kongsbreen, Kronebreen, Infantonna, Kongsvegen and Sidevegen (from north to south). The latter four glaciers were grouped into the Kronebreen glacier complex. The initial glacier geometry is provided by Randolph glacier inventory, (RGI Version 6.0). Surface elevation is derived from the Copernicus DEM, and ice thickness and velocity data are taken from Millan et al. (2022). IGM allows the data download for multiple initial parameters including initial DEM, observed velocity and thickness using the OGGM-shop module. The surface mass balance parameters (z_{ELA}, β_{abl}, and β_{acc}) are identical to those prescribed for the synthetic domain.

Among the selected glaciers, Kronebreen and Kongsbreen are the two major and largest outlet glaciers. Kronebreen is one of the fast-flowing glaciers in the Svalbard archipelago (Schellenberger et al., 2015). The glacier terminus ends in a deep fjord with water depth near the terminus of 50 to 60 m, with a retrograde bed slope. The glacier terminus was relatively stable until 2007 and has been retreating faster since then (Luckman et al., 2015; Schellenberger et al., 2015). The other glacier, Kongsbreen, features two calving fronts oriented northward and southward. The northern branch ends in a deep fjord and has undergone a pronounced retreat, while the southern branch is partially land terminating and has minimal terminus change since 2000. The calving front of the northern branch is 2.1 km wide and has retreated over 3 km in the last two decades (Fig. 3).

2.3.2 Model Calibration

To reproduce the observed near-frontal velocity field of the selected glaciers with IGM, we applied a manual calibration of the friction coefficient. Although IGM includes a data assimilation framework for inferring basal friction, the primary focus of this study is on calving-front evolution rather than optimizing basal sliding through formal inversion. The manual calibration strategy aimed to reproduce the observed frontal velocities derived from the dataset of Millan et al. (2022), which range between 800 to 1200 m a $^{-1}$ at the glacier front. Through iterative testing of different spatial distributions of friction coefficients, we selected spatially varying friction coefficient values that yielded near frontal velocities exceeding 1200 m a $^{-1}$, consistent with the upper range of observed values. In regions where the bed topography is less than zero, a friction coefficient value of 10^{-6} m MPa^{-3} a $^{-1}$ is used, to allow enhanced basal sliding. Further up the glacier, the value increases to 0.04 m MPa^{-3} a^{-1},

https://doi.org/10.5194/egusphere-2026-508
Preprint. Discussion started: 27 February 2026

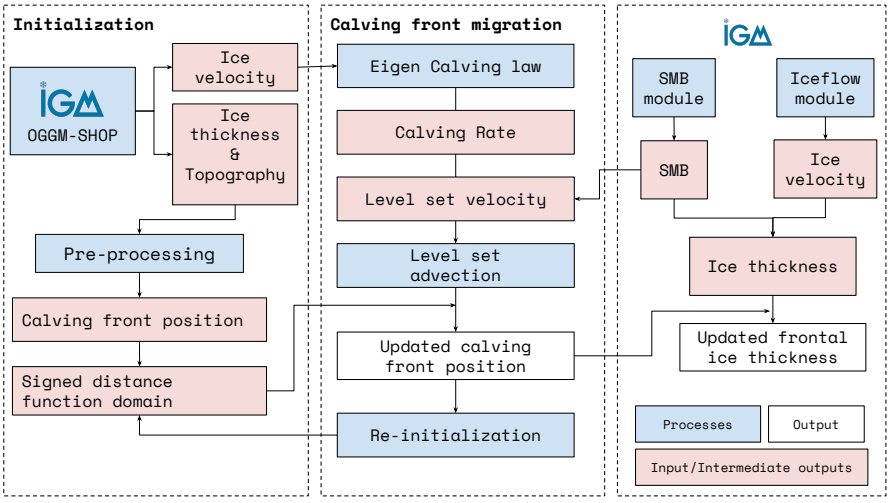

Figure 2. Workflow showing integration of calving framework with IGM for real-world experiments.

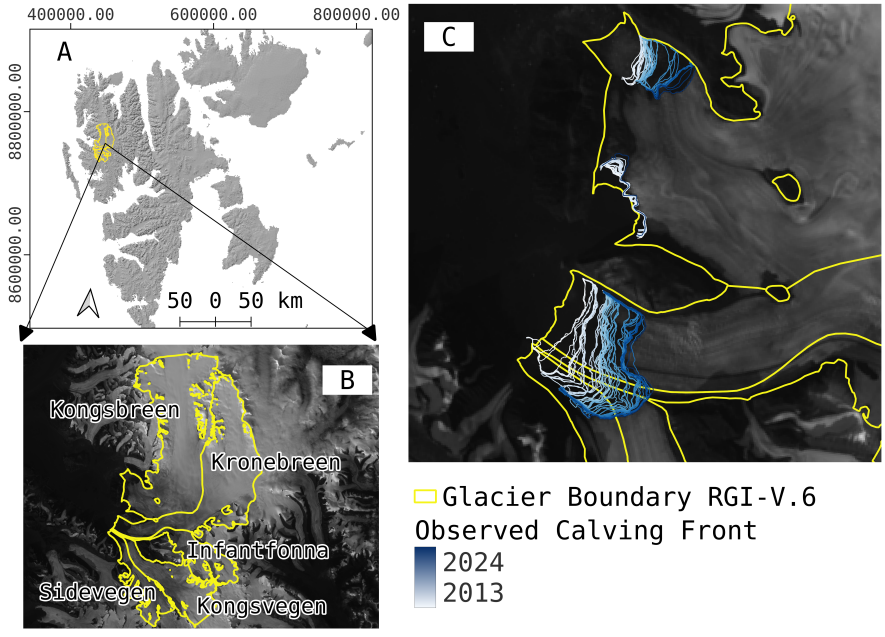

Figure 3. (A) Location of the selected tidewater glaciers in northwestern Svalbard; (B) glacier boundaries (yellow) from the Randolph Glacier Inventory V-6; (C) observed calving front retreat from 2013 and 2024, overlaid on a Sentinel 2 image from September 2024.

https://doi.org/10.5194/egusphere-2026-508
Preprint. Discussion started: 27 February 2026

representing stronger basal resistance. After this inversion, a 10 year relaxation run is pursued with a constant thickness field. After this initialization procedure, we allow the calving front position to evolve in time in line with the calving law defined in Eq. 6

The calving law constant (K_{ec}) is calibrated with observed front position data of Kronebreen, Infantonna, and Sidevegen. The observed calving fronts are obtained using the automated rectilinear box tool of Loebel et al. (2024). The model uses the orthorectified and radiometrically calibrated Level-1 data product of Landsat-8 to generate the calving front positions. For each year of data, the image corresponding to the latest date in September is used for calibration, which acts as a proxy for the end of summer calving front. The calving fronts are then manually readjusted based on high-resolution Sentinel 2 data for improved accuracy. The calibration period is divided into two sections: 2000-2013 and 2013-2024. For the first subperiod, calving front positions are available only for two years, whereas for the second period, annual calving front positions are available. The calibration target is to determine a single K_{ec} value, which best explains the average retreat during a specific period. For the period 2000–2013 the value of K_{ec} is 0.56*10^4 ma^{-1} while for the period 2013-2024 it is 2.3 *10^4 ma^{-1} .

3 Results

Here we present the results of the calving front evolution of the synthetic glacier domain and the real-world experiment. The synthetic experiment use constant values of level set velocity (v_f), while the real-world setup uses level-set velocity estimated from the calving rate and glacier ice velocity (Eq. 4).

3.1 Synthetic glacier domain

Using the synthetic glacier setup, we aim at reproducing physically consistent thinning and thickening during calving front evolution. In this experiment, there is no direct link between IGM velocity and the ice-front velocity, which is prescribed as a constant. However, the IGM derived thickness and ice velocity are updated based on the evolving calving front position. Away from the calving front, IGM updates the geometry according to mass conservation (Eq. 1). The evolution of calving front positions during the advance-retreat phases are given in Fig. 4A. During the advance phase, the front moves 400 m every year, consistent with the prescribed velocity applied to satisfy Eq. 3. The calving front maintains its shape throughout the experiment. During the first half of the retreat phase, the calving front retreats inland, while retracing the previous advance glacier front positions. Subsequent retreat continue until the glacier becomes land-terminating (above 0 m a. s. l.), and iceberg calving is no longer possible.

As the front propagates into the ocean, the newly evolved front maintains a realistic thickness with no step-changes in thickness. The thickness evolution along the centerline of the synthetic glacier domain shows that the front-thickness remains constant during advance phase. During retreat, the glacier area is adjusted according to the position of zero level set. The retreat initially removes the glacier mass gained by the domain during the advance phase, until it reaches the initial extent (Fig. 4B). In addition to retracing front positions, the method also ensures that the frontal thickness is preserved throughout the calving process. During the later retreat phase, ice thickness is removed progressively from the initial glacier extent based on calving

https://doi.org/10.5194/egusphere-2026-508
Preprint. Discussion started: 27 February 2026

front positions. Throughout the experiment, the symmetrical distribution of thickness and surface elevation of the domain is preserved.

IGM seamlessly adjusts the glacier velocities with the evolving glacier geometry. The ice velocity is notably low at the front during the advance phase and first half of the retreat phase. This front of the synthetic glacier domain is characterized by lower ice thickness and slope and high friction coefficient. This reduces the driving stress and explains the slow frontal velocity. The frontal velocity increases considerably later, as the front retreats further, consistent with increase in slope and ice thickness. In contrast, the upstream velocity steadily increases throughout the experiment, since controlling parameters allows velocity buildup (Fig. 4C).

3.2 Real-world Experiment

All the glaciers selected in this study experienced sustained calving throughout the study period, which the model was able to reproduce. The modeled calving fronts (2000-2024) of both glacier complexes are shown in Fig. 5. In the first calibration phase (2000 - 2013), the modeled calving front positions of Kronebreen complex shows a slow retreat and a uniform low calving rate (Fig. 5A). An exception to this is the Sidevegen glacier (Fig. 5A), which exhibits a stable calving front during this period. The Sidevegen calving front is sitting on small ridge ∼50 m. a. s. l, and is initially not controlled by the calving module. The calving front starts to retreat from 2014 onward, owing to huge mass loss at the front and increased calving rate. For Kongsbreen, the modeled glacier front is stable for the period 2000 to 2003, as the frontal velocities and calving rates are low. From 2003 until 2013, the northern front exhibits a steady and smooth retreat until 2013 (Fig. 5B). The front positions in 2013 match well with the observed data for the northern branch. However, the modeled calving front of the southern branch is retreating somewhat faster than the observed data.

In the second calibration phase (2014-2024), the calving front is retreating faster for both glaciers. The modeled calving front matches well with the observed front positions of Kronebreen, Infantfonna, and Kongsvegen glaciers. For Sidevegen, the modeled front propagation is slower than the observed. The model also captures the increased retreat observed along the deeper parts of the Kronebreen complex. This increase in calving rate from 2014 is modeled in Kongsbreen glacier as well. Comparison between observed and modeled front indicates that the calving front is only partially captured, especially at the north front. At the northern front, the modeled calving front shows faster retreat for the eastern section while slower retreat for western section. The southern front of the glacier is relatively stable based on the observed data. The modeled results show similar pattern with no or very slow retreat (Fig. 5B).

4 Discussion

4.1 Numerical stability of the LSM ice-front tracking

The numerical stability of the LSM is tested using a circular and a synthetic glacier domain. The contributor to the numerical inconsistencies of the level set advection mainly comes from a lack of re-initialization and velocity extensions (Sussman

https://doi.org/10.5194/egusphere-2026-508
Preprint. Discussion started: 27 February 2026

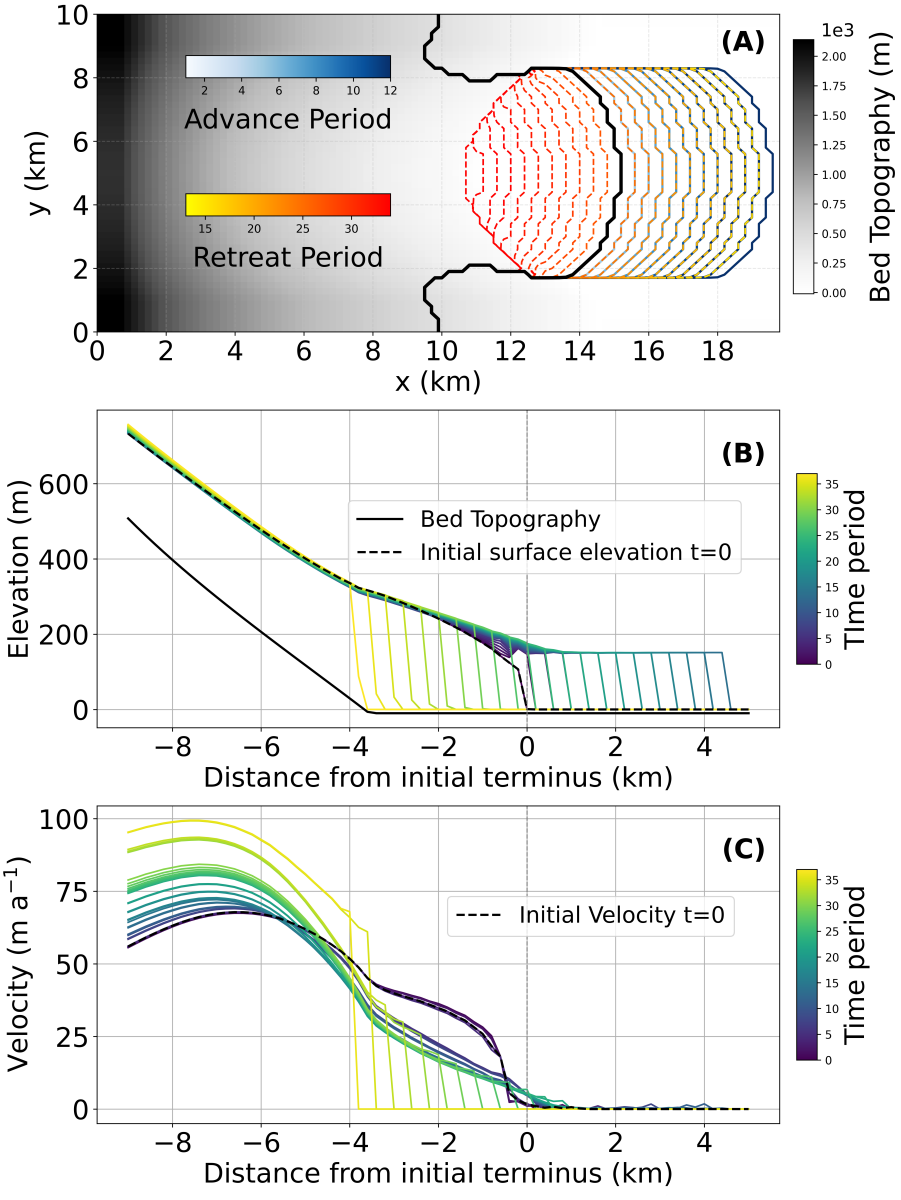

Figure 4. (A) Calving front positions of the synthetic glacier domain over time, with initial terminus position given as the black solid line; (B) glacier surface topography and (C) ice velocity distribution along the flowline.

https://doi.org/10.5194/egusphere-2026-508
Preprint. Discussion started: 27 February 2026

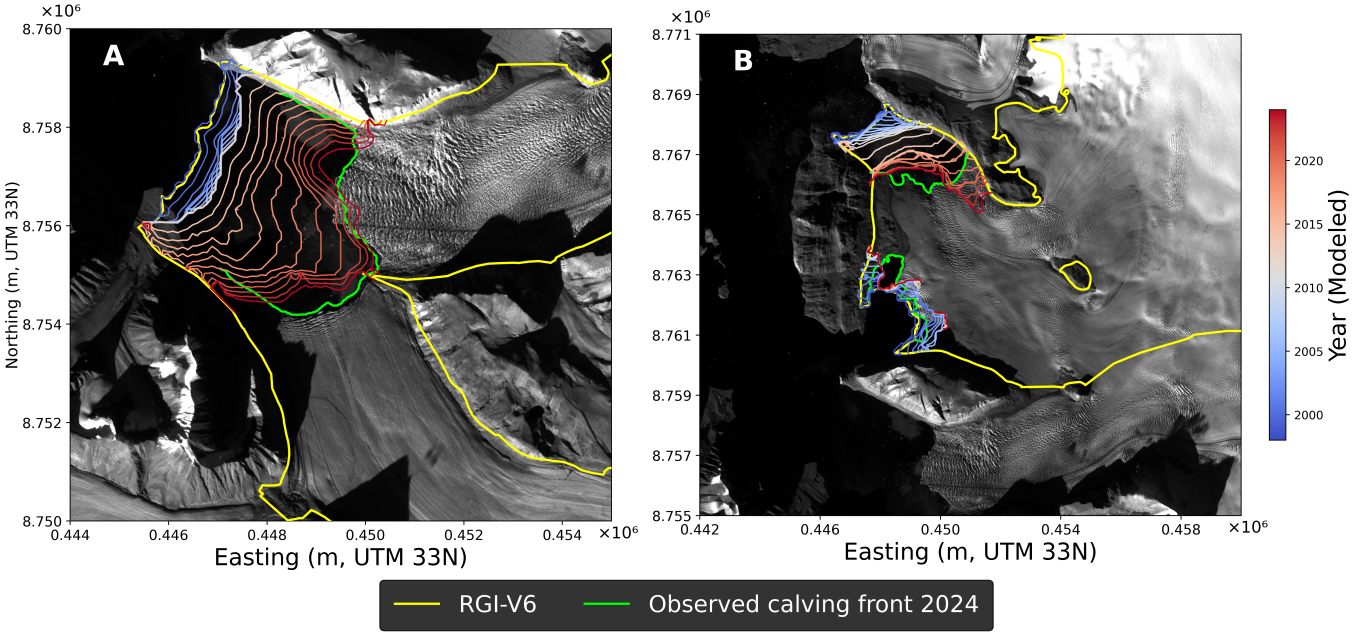

Figure 5. Modeled glacier calving front evolution of Kronebreen complex (A) and Kongsvegen (B) from 2000 to 2024. The initial glacier boundary is given in solid yellow line and the observed calving front for the period 2024 are given as solid green line and the colorbar shows the modeled calving front positions.

et al., 1994). The re-initialization helps to preserve the exact position of the interface as well as the signed distance function (Bondzio et al., 2016). We rely on a partial difference equation-based re-initialization for our finite difference approach. This contributes to a numerically consistent interface evolution by controlling gradient distortion of the LSF. This in turn ensures mass conservation and curvature preservation as evident from the circular interface evolution Fig. A1A and the synthetic glacier front evolution Fig. 4. The re-initialization frequency does not appear to have any significant effect on the accuracy of our model, in contrast to the previous findings by Cheng et al. (2024). This could likely stem either from the relatively small velocities or from the simplicity of the test domain. However, without re-initialization, numerical errors accumulate during level-set advection, leading to increased deviation from analytical solutions. A key requirement for level-set-based calving models is the ability to simulate reversible calving-front migration, along with physically consistent frontal ice thickness update. The synthetic glacier experiments indicate that introducing additional geometric and physical complexities through inclusion of spatially varying ice thickness, an ocean interface and a grounding line, does not compromise the numerical stability of the level set formulation. Instead, the model continues to exhibit isotropic level-set advection, with front propagation remaining independent of the interface geometry and domain orientation. As for the frontal ice thickness, the calving front thickness remains consistent with the initial frontal ice thickness distribution during both advance and retreat phase. No artificial discontinuities are observed in either ice thickness or ice velocity particularly at the calving front. This demonstrates that the method can seamlessly incorporate the geometry update and position-based thickness update within IGM. Furthermore, the

https://doi.org/10.5194/egusphere-2026-508
Preprint. Discussion started: 27 February 2026

initial geometry, bed topography, calving front thickness, and level set velocities are fully controlled in the synthetic glacier domain. This makes it easier to isolate the numerical behavior of level set advection from the physical complexities.

4.2 Glacier calving front evolution on Svalbard

The level set function controls the migration of the ice/water interface whilst it is not employed for the ice-land/ice-free interface. Advance and retreat on land are controlled by the classical mass conservation equation. The real-world setup shows the ability of the method to reproduce the observed calving front migration. In particular, the level set framework allows the calving front to evolve freely, enabling the method to handle the complex topology of the glacier terminus. As shown in the southern branch of Kongsbreen, the model can effectively capture the splitting of the calving front and can treat the zero level set as multiple individual fragments (Fig. 5 B). In addition, the calving-front positions of neighboring glaciers can be simulated simultaneously. This is particularly important where glaciers share a calving front, as their dynamics influence each other.

The accuracy of calving front evolution depends on the choice of calving law and the terminus velocity. The patterns of ice-front retreat are influenced by the calving laws (Choi et al., 2018). They show that the available rate-based calving laws require careful calibration in real-world application. Here we opted for the eigen calving variant. To better capture the temporal patterns of retreat, the calibration period is divided into two decades, the first half with modest retreat rates and a subsequent decade with markedly faster retreat. The modest variations in annual patterns of observed and modeled calving front positions show the difficulty in capturing the short-term forcings with a constant calibration parameter. While the calving parameter cannot be transferred between the two periods, spatial transferability across nearby glaciers remains possible. The calibration values inferred from Kronebreen, Infantonna, and Kongsvegen remain effective when applied on Sidevegen and Kongsbreen, despite differences in geometric confinement. Also, the single proportionality constant was able to reproduce the effect of pinning points and strain rate heterogeneity of most of the calving front positions in Kronebreen complex. The annual patterns of the modeled calving front migration are also controlled by the temporal evolution of glacier ice velocity. Although the model was initially calibrated, we observe that the glacier ice velocity reduces significantly over time. The lower glacier ice velocity also reduces the strain rate based calving rates, forcing the calving front migration to stabilize over time. Consequently, in both glacier setups, the glacier front slows or stabilizes toward the end of the first calibration period.

The glacier front retreat also shows considerable sensitivity to the bed topography as observed in other calving model applications (Morlighem et al., 2016; Choi et al., 2018). The glacier retreat is faster along the retrograde bed sections, and is more in agreement with observations. Within the Kronebreen complex, eigen calving performs well at retrograde front positions. The fast flow typical of retrograde slope regions produces high along-flow strain rates and negligible or weak across-flow strain rates. This reduces the noise in the overall calving rate, making the eigen calving suitable for application on fast-flowing glaciers of Svalbard. Although eigen calving law is appropriate for unconfined ice domains (Levermann et al., 2012; Wilner et al., 2023), a comparative modeling study in the Greenland fjords has shown that eigen calving performs poorly where flow is constrained by narrow, near-parallel valley walls (Choi et al., 2018). Kongsbreen shares a similar geometric confinement. where the calving front is bounded by small ridges and narrow lateral valleys. This adds additional noise to the strain rates, which affects the pattern and magnitude of the calving rate. Kongsbreen continues to have lower frontal velocity

https://doi.org/10.5194/egusphere-2026-508
Preprint. Discussion started: 27 February 2026

and thickness until 2015, irrespective of calving perturbations. However, prolonged faster calving has increased the local speed up of glaciers near the terminus and results in accelerated calving at the western margin of the south front. Another contributing factor to the mismatch between observed and modeled front positions is the spatial patterns of IGM-derived glacier ice velocity. Although the modeled and observed velocities agree well at the beginning of the simulation, the discrepancies grow over time. As the current scope of our study does not include a full reconstruction of glacier velocity fields, we rely on IGM-solver-derived velocities. For future application, we recommend a more realistic velocity simulation using the IGM-inversion.

4.3 Potential and limitations

The MALT glaciers represent a substantial fraction of the global glacier area and ice volume. Their direct contact with water introduces additional dynamic and thermodynamic forcings that can trigger phases of rapid frontal retreat and enhanced ice discharge. Recent studies have extended sheet models such as ISSM, Úa and Elmer/Ice by incorporating the LSM to enable the calving-front migration of ice-sheets and water-terminating glaciers (Bondzio et al., 2016; Cheng et al., 2024; Badgeley et al., 2025; Barnes et al., 2026). These studies enable a physically consistent simulations of the calving-front retreat at glacier to regional-scales. These implementations are typically embedded within finite element frameworks. In contrast, IGM is based on a structured grid architecture. The current implementation introduces sub-grid level-set implementation within the IGM framework allowing calving-front migration to be resolved below the native grid spacing. This approach provides a geometrically consistent representation of calving-front evolution while preserving the computational efficiency of IGM. Although the current implementation is mainly tested on marine-terminating glaciers, it is equally applicable to any water-terminating glacier, including lake-terminating glaciers. However, it is assumed that the entire setup fully remain grounded as it advances into the ocean. This simplification limits the application of the model for investigating calving-front flotation.

In the present study, sub-aqueous melt is not explicitly included. The omission of submarine melt represents a simplification of the frontal mass balance. The modeled retreat should therefore be interpreted as the response to stress-driven calving alone. Further inclusion of sub-aqueous melt could explain the spatial variability in calving front migration of the selected glaciers accurately. However, isolating stress-based calving allows us to evaluate the numerical implementation of sub-grid calving-front migration within the IGM framework without introducing additional uncertainties. Furthermore, the current modeling framework employs a simplified strain-based calving scheme to study calving dynamics. Incorporating more physics-based calving mechanisms would likely enhance the predictive capability of the model and better reflect the diversity of calving processes observed across tidewater and lake-terminating glaciers. The modular nature of the implemented level-set scheme offers flexibility to incorporate multiple calving laws. Lastly, the application of the method to real-world settings reveals a strong sensitivity to the calving parameter, which governs the magnitude of the calving rate. This sensitivity underscores the necessity for glacier-specific calibration strategies to constrain calving behavior. However, such calibration can be computationally intensive and time-consuming.

https://doi.org/10.5194/egusphere-2026-508
Preprint. Discussion started: 27 February 2026

5 Conclusions

In this study, we present the implementation and integration of a fully-coupled calving module into the Instructed Glacier Model (IGM). The module comprises subgrid tracking of the glacier front using the level-set method and an eigen-calving law. The subgrid tracking captures the dynamically evolving calving front, while the eigen calving law links frontal migration directly to ice-dynamic strain-rate re-adjustments within the glacier. The initial testing of the model on the synthetic domain shows promise as a tool for accurately simulating the ice fronts of grounded glacier tongues. The synthetic experiment also assesses the reversibility and shape preservation of the level set function, demonstrating that the calving front can advance and retreat without introducing numerical artifacts or distortions in its geometry. As the position of the calving front can strongly affect the ice stress regime and velocity, it is critical to capture the subtle frontal positions. Unlike traditional grid-based simulations, where calving occurs only at discrete resolution-defined intervals, the LSM enables continuous tracking of calving front evolution within grid cells. This subgrid representation is found to effectively preserve curvature, local orientation, and boundary continuity at the terminus. As a result, the model captures the subtleties of glacier advance and retreat more realistically.

The real-world applicability of the model was tested on five glaciers in Svalbard. These include the Kronebereen complex and the Kongsbreen. Although the algorithm effectively reproduces the general trends and patterns of the calving fronts, it is also highly sensitive to changes in the calibration strategy. The accuracy of the modeled calving front migration depends on an appropriate calibration of the calving parameter, on reliable basal topography, and consistency between modeled and observed velocities. Future work should explore integrating adaptive or time-dependent parameter calibration techniques, potentially leveraging data assimilation frameworks or observational constraints (Hossain et al., 2023; Herrmann et al., 2025). These enhancements were beyond the scope of the present model development.

Code availability. All glacier datasets used in this analysis are freely available at https://cluster.klima.uni-bremen.de/data/gdirs/dems_v2/default/RGI62/b_010/L1/. The Instructed Glacier Model (IGM) is open source and can be accessed at https://github.com/instructed-glacier-model/igm. The level set function implementation used in this study was adopted from Kori-ULB ice flow model, available at https://github.com/FrankPat/Kori-ULB/blob/main/subroutines/LSFfunction.m.

*Author contributions.*VP and JJF designed and conceptualized the experiments. VP implemented the numerical modeling simulations. JJF, IT, ARG, OH and MKC contributed to the discussion on the model implementation. VP wrote the manuscript and created the figures. JJF, ARG, OH, MKC, JRJ, IT and GJ reviewed and edited the manuscript.

Competing interests. The authors have the following competing interests: JJF is a member of the editorial board of The Cryosphere.

Acknowledgements. VP, OH,ARG, and JJF received funding from the European Union's Horizon 2020 research and innovation programme via the European Research Council (ERC) as a Starting Grant (FRAGILE project) under grant Agreement No.

https://doi.org/10.5194/egusphere-2026-508
Preprint. Discussion started: 27 February 2026

948290. IT was supported by DFG Individual Research Grant project RESPONSE (No. 495516510). MKC is funded through the International Doctoral Program 'Measuring and Modeling Mountain Glaciers and Ice Caps in a Changing Climate' (M3OCCA) funded by the Bavarian State Ministry of Science and Arts under the Elite Network Bavaria. The authors thankfully acknowledge the scientific support and HPC resources provided by the Erlangen National High Performance Computing Center (NHR@FAU) of the Friedrich-Alexander-Universität Erlangen-Nürnberg (FAU). NHR funding is provided by federal and Bavarian state authorities. NHR@FAU hardware is partially funded by the German Research Foundation (DFG) (No. 440719683). We gratefully thank Frank Pattyn for making the level set code publicly available via Github. During the preparation of this manuscript, the author used ChatGPT 4.0, an AI-assisted editing tool, to improve spelling, grammar, clarity, and readability.

Appendix A

We present a simple test setup used to test the sanity of our LSM implementation and ability of the model to preserve mass and shape of the interface. For these simulations coupling with IGM was not required. We used a square-shaped domain of size 500 x 500 m, with a resolution of 10 m. The domain is divided into a negative and a positive region by a circular interface. The value of ϕ is initialized using a fast marching approach, considering the interface as zero.

For level set advection, the test domain is advanced with constant level set velocity (v_f) of 20 m a^{-1} in both the x and y directions on the interface. The level set is advected for a period of 5 years with time steps following the Courant-Friedrichs-Lewy criteria. With a Courant-Friedrichs-Lewy-constrained time step, the interface advances at a distance smaller than the grid spacing of 10 m. This ensures that the calving front evolves at subgrid scales, providing a direct test of the level-set method's ability to track continuous front positions. Two numerical experiments are conducted on this setup. In the first, level set function is re-initialized each time step whilst the second is without re-initialization. The modeled interface evolution of the circular domain is compared with an analytical solution of the imposed rate of front migration to test the ability of the LSM to reproduce the same rate of interface migration (Fig. A1). The circular interface evolves consistently with the analytical solution of the domain (Fig. A1A). The level set advection (Eq. 3) here is coupled with re-initialization (Eq. 7) of the level set field and velocity extension (Eq. 5). This approach to interface evolution captures the orientation and magnitude of the level set velocity, while preserving the shape and initial mass of the domain. In contrast, the classical level set solution (Eq. 3) lacks a re-initialization and velocity extension. The classic method thus fails to preserve the mass and curvature of the interface. The disagreement in analytical and classic level set advection is given in Fig. A1B. However, the magnitude and orientation of the interface velocity are maintained to an extent in the experiment. This could potentially change based on the complexity of the interface, which is why re-initialization is recommend for level set advection. Since the circular domain contains no ice thickness or ice velocity information, the experiment is limited to assessing the influence of level set velocity on the orientation of calving front/model domain, magnitude, and degree of mass conservation. The circular synthetic setup lack the necessary geometric and dynamical ice-flow parameter to test the model performance.

https://doi.org/10.5194/egusphere-2026-508
Preprint. Discussion started: 27 February 2026

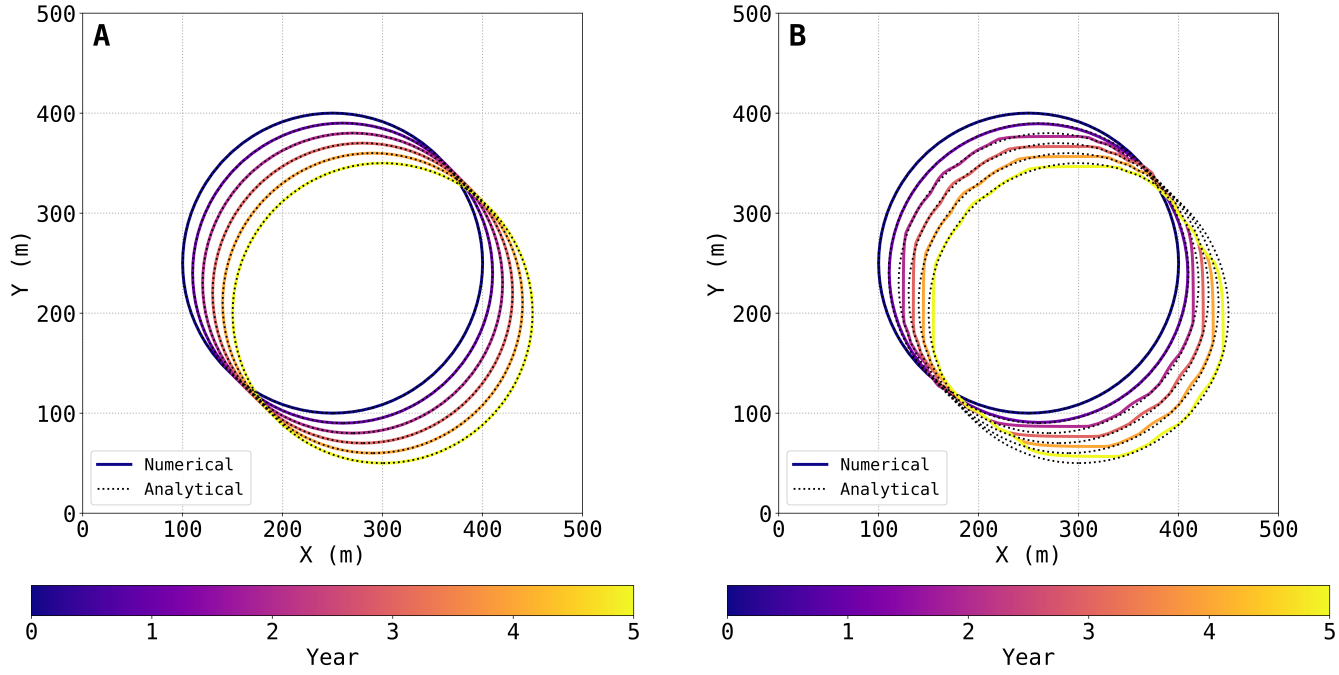

Figure A1. Interface evolution of a circular domain with re-initialization (A) and without re-initialization (B). The interface evolution from current implementation are given as the colored contours while the analytical shift of zero-interface is given as black dashed lines.

References

Adalsteinsson, D. and Sethian, J. A.: The Fast Construction of Extension Velocities in Level Set Methods, Journal of Computational Physics, 148, 1999.

Amundson, J. M., Truffer, M., and Zwinger, T.: Tidewater glacier response to individual calving events, Journal of Glaciology, 68, 1117–1126, https://doi.org/10.1017/jog.2022.26, 2022.

Badgeley, J. A., Morlighem, M., and Seroussi, H.: Increased sea-level contribution from northwestern Greenland for models that reproduce observations, Proceedings of the National Academy of Sciences, 122, e2411904 122, https://doi.org/10.1073/pnas.2411904122, 2025.

Barnes, J. M., Gudmundsson, G. H., Goldberg, D. N., and Sun, S.: Modelling the sensitivity of ice loss to calving front retreat rates in the Amundsen Sea Embayment, West Antarctica, The Cryosphere, 20, 777–790, https://doi.org/10.5194/tc-20-777-2026, 2026.

Benn, D. I., Warren, C. R., and Mottram, R. H.: Calving processes and the dynamics of calving glaciers, Earth-Science Reviews, 82, 143–179, https://doi.org/10.1016/j.earscirev.2007.02.002, 2007.

Bondzio, J. H., Seroussi, H., Morlighem, M., Kleiner, T., Rückamp, M., Humbert, A., and Larour, E. Y.: Modelling calving front dynamics using a level-set method: application to Jakobshavn Isbræ, West Greenland, The Cryosphere, 10, 497–510, https://doi.org/10.5194/tc-10-497-2016, 2016.

Brown, C. S., Meier, M. F., and Post, A.: Calving speed of Alaska tidewater glaciers, with application to Columbia Glacier, Tech. Rep. 1258 C, U.S. Geological Survey Professional Paper, https://doi.org/10.3133/pp1258c, 1983.

https://doi.org/10.5194/egusphere-2026-508
Preprint. Discussion started: 27 February 2026

Cheng, G., Morlighem, M., and Gudmundsson, G. H.: Numerical stabilization methods for level-set-based ice front migration, Geoscientific Model Development, 17, 6227–6247, https://doi.org/10.5194/gmd-17-6227-2024, 2024.

Choi, Y., Morlighem, M., Wood, M., and Bondzio, J. H.: Comparison of four calving laws to model Greenland outlet glaciers, The Cryosphere, 12, 3735–3746, https://doi.org/10.5194/tc-12-3735-2018, 2018.

Cogley, J. G., Arendt, A. A., Bauder, A., Braithwaite, R. J., Hock, R., Jansson, P., Kaser, G., Möller, M., Nicholson, L., Rasmussen, L. A., and Zemp, M.: Glossary of glacier mass balance and related terms, Tech. rep., International Hydrological Programme, UNESCO, Paris, 2010.

Compagno, L., Huss, M., Zekollari, H., Miles, E. S., and Farinotti, D.: Future growth and decline of high mountain Asia's ice-dammed lakes and associated risk, Communications Earth & Environment, 3, 191, https://doi.org/10.1038/s43247-022-00520-8, 2022.

Coulon, V., Klose, A. K., Kittel, C., Edwards, T., Turner, F., Winkelmann, R., and Pattyn, F.: Disentangling the drivers of future Antarctic ice loss with a historically calibrated ice-sheet model, The Cryosphere, 18, 653–681, https://doi.org/10.5194/tc-18-653-2024, 2024.

Dussaillant, I., Hugonnet, R., Huss, M., Berthier, E., Bannwart, J., Paul, F., and Zemp, M.: Annual mass change of the world's glaciers from 1976 to 2024 by temporal downscaling of satellite data with in situ observations, Earth System Science Data, 17, 1977–2006, https://doi.org/10.5194/essd-17-1977-2025, 2025.

Fürst, J. J., Farías-Barahona, D., Blindow, N., Casassa, G., Gacitúa, G., Koppes, M., Lodolo, E., Millan, R., Minowa, M., Mouginot, J., Ptlicki, M., Rignot, E., Rivera, A., Skvarca, P., Stuefer, M., Sugiyama, S., Uribe, J., Zamora, R., Braun, M. H., Gillet-Chaulet, F., Malz, P., Meier, W. J.-H., and Schaefer, M.: The foundations of the Patagonian icefields, Communications Earth & Environment, 5, 142, https://doi.org/10.1038/s43247-023-01193-7, 2024.

GlaMBIE Team: Community estimate of global glacier mass changes from 2000 to 2023, Nature, https://doi.org/10.1038/s41586-024-08545-z, 2025.

Herrmann, O., Groos, A. R., Tabone, I., Jouvet, G., and Fürst, J. J.: A Kalman filter-based framework for assimilating remote sensing observations into a surface mass balance model, Annals of Glaciology, 66, e23, https://doi.org/10.1017/aog.2025.10020, 2025.

Hossain, M. A., Pimentel, S., and Stockie, J. M.: Simulating surface height and terminus position for marine outlet glaciers using a level set method with data assimilation, Journal of Computational Physics, 474, 111 766, https://doi.org/https://doi.org/10.1016/j.jcp.2022.111766, 2023.

Hugonnet, R., McNabb, R., Berthier, E., et al.: Accelerated global glacier mass loss in the early twenty-first century, Nature, 592, 726–731, https://doi.org/10.1038/s41586-021-03436-z, 2021.

Jouvet, G., Cordonnier, G., Kim, B., Lüthi, M., Vieli, A., and Aschwanden, A.: Deep learning speeds up ice flow modelling by several orders of magnitude, Journal of Glaciology, 68, 651–664, https://doi.org/10.1017/jog.2021.120, 2022.

Kochtitzky, W. H., Truffer, M., and Arendt, A. A.: Exploring the impact of a frontal ablation parameterization on projected 21st-century mass change for Northern Hemisphere glaciers, Journal of Glaciology, 68, 1–13, https://doi.org/10.1017/jog.2022.5, 2022a.

Kochtitzky, W. H., Truffer, M., and Arendt, A. A.: The unquantified mass loss of Northern Hemisphere marine-terminating glaciers, Nature Communications, 13, 1–10, https://doi.org/10.1038/s41467-022-33231-x, 2022b.

Kochtitzky, W. H., Truffer, M., and Arendt, A. A.: Frontal Ablation of Every Greenlandic Glacier From 2000 to 2020, Geophysical Research Letters, 50, e2023GL104 095, https://doi.org/10.1029/2023GL104095, 2023.

Levermann, A., Albrecht, T., Winkelmann, R., Martin, M. A., Haseloff, M., and Joughin, I.: Kinematic first-order calving law implies potential for abrupt ice-shelf retreat, The Cryosphere, 6, 273–286, https://doi.org/10.5194/tc-6-273-2012, 2012.

https://doi.org/10.5194/egusphere-2026-508
Preprint. Discussion started: 27 February 2026

Li, D., DeConto, R. M., and Pollard, D.: Climate model differences contribute deep uncertainty in future Antarctic ice loss, Science Advances, 9, eadd7082, https://doi.org/10.1126/sciadv.add7082, 2023.

Loebel, E., Scheinert, M., Horwath, M., Humbert, A., Sohn, J., Heidler, K., Liebezeit, C., and Zhu, X. X.: Calving front monitoring at a subseasonal resolution: a deep learning application for Greenland glaciers, The Cryosphere, 18, 3315–3332, https://doi.org/10.5194/tc-18-3315-2024, 2024.

Luckman, A., Benn, D. I., Cottier, F., Bevan, S., Nilsen, F., and Inall, M.: Calving rates at tidewater glaciers vary strongly with ocean temperature, Nature Communications, 6, 8566, https://doi.org/10.1038/ncomms9566, 2015.

Martin, M. A., Winkelmann, R., Haseloff, M., Albrecht, T., Bueler, E., Khroulev, C., and Levermann, A.: The Potsdam Parallel Ice Sheet Model (PISM-PIK) – Part 2: Dynamic equilibrium simulation of the Antarctic ice sheet, The Cryosphere, 5, 727–740, https://doi.org/10.5194/tc-5-727-2011, © Author(s) 2011. CC Attribution 3.0 License, 2011.

Millan, R., Mouginot, J., Rabatel, A., and Morlighem, M.: Ice velocity and thickness of the world's glaciers, Nature Geoscience, 15, 124–129, https://doi.org/10.1038/s41561-021-00885-z, 2022.

Minowa, M., Schaefer, M., and Skvarca, P.: Effects of topography on dynamics and mass loss of lake-terminating glaciers in southern Patagonia, Journal of Glaciology, 69, 1580–1597, https://doi.org/10.1017/jog.2023.42, 2023.

Mitcham, T., Gudmundsson, G. H., and Bamber, J. L.: The instantaneous impact of calving and thinning on the Larsen C Ice Shelf, The Cryosphere, 16, 883–901, https://doi.org/10.5194/tc-16-883-2022, 2022.

Morlighem, M., Bondzio, J., Seroussi, H., Rignot, E., Larour, E., Humbert, A., and Rebuffi, S.: Modeling of Store Gletscher's calving dynamics, West Greenland, in response to ocean thermal forcing, Geophysical Research Letters, 43, 2659–2666, https://doi.org/10.1002/2016GL067695, 2016.

Mouginot, J., Rignot, E., Bjørk, A. A., Wood, M., et al.: Forty-six years of Greenland Ice Sheet mass balance from 1972 to 2018, Proceedings of the National Academy of Sciences, 116, 9239–9244, https://doi.org/10.1073/pnas.1904242116, 2019.

Nick, F. M., Vieli, A., Howat, I. M., and Joughin, I.: Large-Scale Changes in Greenland Outlet Glacier Dynamics Triggered at the Terminus, Nature Geoscience, 2, 110–114, https://doi.org/10.1038/ngeo394, 2009.

Nick, F. M., Vieli, A., Howat, I. M., and Joughin, I.: Future sea-level rise from Greenland's main outlet glaciers in a warming climate, Nature, 497, 235–238, https://doi.org/10.1038/nature12146, 2013.

Nuth, C., Moholdt, G., Kohler, J., Hagen, J. O., and Kääb, A.: Svalbard Glacier Elevation Changes and Contribution to Sea Level Rise, Journal of Geophysical Research: Earth Surface, 115, https://doi.org/10.1029/2008JF001223, 2010.

Osher, S. and Sethian, J. A.: Fronts propagating with curvature-dependent speed: Algorithms based on Hamilton–Jacobi formulations, Journal of Computational Physics, 79, 12–49, https://doi.org/10.1016/0021-9991(88)90002-2, 1988.

Pattyn, F.: Sea-level response to melting of Antarctic ice shelves on multi-centennial timescales with the fast Elementary Thermomechanical Ice Sheet model (f.ETISh v1.0), The Cryosphere, 11, 1851–1878, https://doi.org/10.5194/tc-11-1851-2017, 2017.

Pfeffer, W., Dyurgerov, M., Kaplan, M., Dwyer, J., Sassolas, C., Jennings, A., Raup, B., and Manley, W.: Numerical modeling of late Glacial Laurentide advance of ice across Hudson Strait: Insights into terrestrial and marine geology, mass balance, and calving flux, Paleoceanography, 12, 97–110, 1997.

Pfeffer, W. T.: Alaskan Glacier beats a dramatic retreat, Eos, Transactions, American Geophysical Union, 81, 577, https://doi.org/10.1029/EO081i048p00577, 2000.

Pope, A., Cogley, J. G., Hock, R., Rasmussen, L. A., Arendt, A. A., Bauder, A., Braithwaite, R. J., Jansson, P., Kaser, G., Möller, M., Nicholson, L., and Zemp, M.: Glossary of Glacier Mass Balance and Related Terms, Polar Record, 48, e15,

https://doi.org/10.5194/egusphere-2026-508
Preprint. Discussion started: 27 February 2026

https://doi.org/10.1017/S0032247411000805, published in: International Hydrological Programme (IHP) of UNESCO, IHP-VII Technical Documents in Hydrology No. 86, IACS Contribution No. 2, UNESCO, Paris, vi + 114 p., 2011, 2012.

Pralong, A. and Funk, M.: A level-set method for modeling the evolution of glacier geometry, Journal of Glaciology, 50, 485–491, https://doi.org/10.3189/172756504781829774, 2004.

Recinos, B., Maussion, F., Rothenpieler, T., and Marzeion, B.: Impact of frontal ablation on the ice thickness estimation of marine-terminating glaciers in Alaska, The Cryosphere, 13, 2657–2672, https://doi.org/10.5194/tc-13-2657-2019, 2019.

Schellenberger, T., Dunse, T., Kääb, A., Kohler, J., and Reijmer, C. H.: Surface speed and frontal ablation of Kronebreen and Kongsbreen, NW Svalbard, from SAR offset tracking, The Cryosphere, 9, 2339–2355, https://doi.org/10.5194/tc-9-2339-2015, 2015.

Schuler, T. V., Benestad, R. E., Isaksen, K., Kierulf, H. P., Kohler, J., Moholdt, G., and Schmidt, L. S.: Svalbard's 2024 Record Summer: An Early View of Arctic Glacier Meltdown?, Proceedings of the National Academy of Sciences of the United States of America, 122, e2503806 122, https://doi.org/10.1073/pnas.2503806122, 2025.

Shugar, D. H., Burr, A., Haritashya, U. K., Kargel, J. S., Watson, C. S., Kennedy, M. C., Bevington, A. R., Betts, R. A., Harrison, S., and Strattman, K.: Rapid worldwide growth of glacial lakes since 1990, Nature Climate Change, 10, 939–945, https://doi.org/10.1038/s41558-020-0855-4, 2020.

Sussman, M., Smereka, P., and Osher, S.: A level set approach for computing solutions to incompressible two-phase flow, Journal of Computational Physics, 114, 146–159, https://doi.org/10.1006/jcph.1994.1155, 1994.

Vacek, F., Nick, F. M., Benn, D., Zwarts, M. P. A., Immerzeel, W., and van de Wal, R. S. W.: Contrasting dynamics of lake- and marine-terminating glaciers under same climatic conditions, EGUsphere, 2025, 1–26, https://doi.org/10.5194/egusphere-2025-5733, 2025.

van der Veen, C.: Tidewater calving, Journal of Glaciology, 42, 375–385, https://doi.org/10.3189/s0022143000004226, 1996.

Vieli, A. and Nick, F. M.: Understanding and modelling rapid dynamic changes of tidewater outlet glaciers: issues and implications, Surveys in Geophysics, 32, 437–458, https://doi.org/10.1007/s10712-011-9132-4, 2011.

Wilner, J. A., Morlighem, M., and Cheng, G.: Evaluation of four calving laws for Antarctic ice shelves, The Cryosphere, 17, 4889–4901, https://doi.org/10.5194/tc-17-4889-2023, 2023.

Wouters, B., Gardner, A. S., and Moholdt, G.: Global glacier mass loss during the GRACE satellite mission (2002–2016), Frontiers in Earth Science, 7, 96, https://doi.org/10.3389/feart.2019.00096, 2019.

Xue, T., Sun, W. C., Adriaenssens, S., Wei, Y., and Liu, C.: A new finite element level set reinitialization method based on the shifted boundary method, Journal of Computational Physics, 438, 110 360, https://doi.org/10.1016/j.jcp.2021.110360, 2021.

Zemp, M., Huss, M., Thibert, E., et al.: Global glacier mass changes and their contributions to sea-level rise from 1961 to 2016, Nature, 568, 382–386, https://doi.org/10.1038/s41586-019-1071-0, 2019.